



Correlating the seismic acceleration of reinforced concrete moment-resisting-frames with structural and earthquake characteristics

Shir Parizat¹ · Ronnie Kamai¹ · Assaf Shmerling¹

Received: 13 December 2023 / Accepted: 3 June 2024 / Published online: 28 June 2024
© The Author(s) 2024

Abstract

Nonstructural components (NSCs) are elements within the building unrelated to the lateral load-carrying system. Failure of NSCs during earthquakes can result in casualties, significant economic losses, disabled critical infrastructures, and loss of building functionality. The NSCs can be categorized into two primary groups: deformation-sensitive and acceleration-sensitive. Thanks to well-established seismic design guidelines and standards, buildings may suffer minor seismic deformations – resulting in lesser damage to deformation-sensitive components. However, planning under the peak floor response or peak floor acceleration (PFA) is getting much less attention – exposing the acceleration-sensitive components to greater risk. This manuscript develops equations for moment-resisting reinforced concrete frames (MRRCFs) that estimate the total floor acceleration. The data is gathered based on 984 inelastic response simulations, elaborated to create an idealized equation based on the earthquake characteristics. The developed equation offers engineers a quantitative approach to understanding the inertial forces applied to the NSCs within the building during earthquakes, allowing them to plan for potential risks due to earthquakes.

Keywords Nonstructural components · Moment-resisting reinforced concrete frames · Total floor acceleration · Ground motions · Earthquake response

1 Introduction

Nonstructural components (NSCs) are elements within the building unrelated to the load-bearing system. In addressing their sensitivity to dynamic loads (i.e., winds and earthquakes), The NSCs are classified into two categories (e.g., ASCE 2000): acceleration-sensitive (e.g., generators, acoustic suspended ceilings, mechanical equipment, and elevators) and deformation-sensitive (e.g., masonry infills and glazing walls). The comprehensive report by

✉ Assaf Shmerling
assafs@bgu.ac.il

¹ Department of Civil and Environmental Engineering, Ben-Gurion University of the Negev, Beer-Sheva, Israel

Taghavi and Miranda (2003), as part of the Pacific Earthquake Engineering Research Center (PEER), underscores the significance of NSCs in maintaining structural serviceability. Extreme damage to NSCs, as elucidated in their study, not only jeopardizes the structure's functionality but can also lead to injuries and substantial economic losses. However, despite numerous methodologies for estimating the seismic response of NSCs since the 1970s, these are not yet incorporated into code provision, as highlighted in a review Wang et al. (2021). Despite the accumulated knowledge, modern building codes have yet to fully integrate these procedures, underscoring the need for further progress in this critical area.

Very few studies investigate the relationship between earthquake properties and the level of seismic accelerations applied to the structure. The research conducted by Elenas and Meskouris (2001) delves into the seismic response analysis of an 8-story reinforced concrete frame structure subjected to 13 different ground motion records. Employing Pearson's and Spearman's correlation coefficients, this study reveals a strong correlation between total acceleration, Arias intensity (I_A), and peak ground velocity (PGV). The study conducted by Reinoso and Miranda (2005) presented results from six instrumented tall buildings, one of which was subjected to four recorded earthquake ground motions. The findings of the structure exposed to four ground motions indicated a positive correlation between structural accelerations and peak ground accelerations (PGA). Nevertheless, it is important to note that this conclusion is based on data from a single structure and only a few records and that no additional ground motion intensity measures (GMIM) were evaluated.

Further supporting the direct connection between PGA and structural acceleration is the study by Kim and White (2004). This study concentrates on a single-story building subjected to four seismic tests with varying maximum input accelerations, emphasizing a positive correlation between PGA and structural accelerations. Similar to the previous study, this study does not explore other GMIMs besides PGA, stressing the need for more comprehensive datasets to enrich our understanding of seismic response characteristics.

In the study by Baker (2007), a linear-elastic analysis was conducted on three structural configurations: one frame structure and two wall structures. The primary aim of this study was to predict the NSC's acceleration demand in response to recorded earthquake ground motions. In achieving their objective, three different GMIMs were considered: equipment relative average spectral acceleration (E-ASAR), PGA, and spectral acceleration at the fundamental frequency ($S_{pa}(f_1)$). The analysis utilized a comprehensive dataset comprising 2,011 records. The study results indicate that PGA is the most reliable GMIM for estimating floor response spectra (FRS) in frame structures, while E-ASAR is a more suitable choice for characterizing FRS in wall structures.

In recent decades, a few equations for estimating multistory building peak floor acceleration (PFA) were proposed in the literature. One of the more notable works is that of Taghavi and Miranda (2004), who analyzed three different structural systems (six-story dual system, 13-story, and 30-story moment-resisting frames) under 80 earthquake records of PGA ranging between 0.03 g and 0.44 g. Their examination refers to small and moderate earthquakes, so the structure is expected to remain in the elastic range. Fathali and Lizundia (2011) propose empirical equations when earthquakes of PGA up to 0.523 g are concerned. The equations stem from the earthquake response of 16 structural systems under 37 earthquake records. They also suggest empirical equations for existing buildings and buildings in their design stage. The NIST (2018) report provides solutions explicitly to improve the seismic performance of NSCs and offers equations for estimating PFA. The equations depend on the

structural characteristics rather than the ground motion parameters and employ earthquake records characterized by PGA greater than 0.20 *g*.

In this paper, we study the correlation between different GMIMs and the structural response regarding total and relative floor acceleration and propose an equation for evaluating the maximum total acceleration of MRRCF systems. We focus on a plane strain analysis of inelastic MRRCF systems at a broad range of fundamental periods (between 0.5 *s* and 4.0 *s*). The eight MRRCFs designed especially for this work will be examined under 123 ground motion time-histories within a broad range of intensities, yielding about 984 inelastic response simulations. The uniqueness of this study lies in the use of nonlinear simulations, coupled with an exploration into the impact of structural characteristics and GMIMs on the total structural acceleration.

2 Dynamic equilibrium and parametric notations

The empirical equations developed in this paper stem from the correlation level between the floor accelerations and the earthquake characteristics. More particularly, we include two different definitions for floor acceleration (relative and total) and five GMIMs. First, we formulate the equation governing the dynamic equilibrium of an MRRCF system subjected to a ground motion. That is:

$$\mathbf{m}\ddot{\mathbf{u}}(t) + \mathbf{c}\dot{\mathbf{u}}(t) + \mathbf{f}^R(t) = -\mathbf{m}1\ddot{u}_g(t) \tag{1}$$

where $\mathbf{u}(t)$ is the relative-to-ground displacement vector, $\dot{\mathbf{u}}(t)$ is the relative velocities vector, $\ddot{\mathbf{u}}(t)$ is the relative accelerations vector, \mathbf{c} is the inherent Caughey damping matrix, 1 is a unity vector, $\ddot{u}_g(t)$ is the ground acceleration, \mathbf{m} is the mass matrix, and $\mathbf{f}^R(t)$ is the inelastic lateral resisting forces vector. The maximum total acceleration is calculated by:

$$\ddot{u}^{t,max} = \max_n \left\{ \max_t |\ddot{\mathbf{u}}^t(t)| \right\} \leftrightarrow \ddot{\mathbf{u}}^t(t) = \ddot{\mathbf{u}}(t) + 1a_g(t) \ , \ \ddot{\mathbf{u}}^t(t) = \begin{Bmatrix} \ddot{u}_1^t(t) \\ \vdots \\ \ddot{u}_N^t(t) \end{Bmatrix} \tag{2}$$

The correlations of $\ddot{u}^{t,max}/\ddot{u}^{r,max}$ and the GMIM, namely PGA, PGV, peak-ground-displacement (PGD), cumulative-absolute-velocity (CAV), and IA, are quantified and elaborated when a high level exists.

Pearson correlation coefficient and Spearman’s rank correlation coefficient are used to quantify the relationship between structural accelerations and earthquake characteristics. Their respective formulas are given by:

$$\rho_{\text{pearson}} = \frac{\sum_{i=1}^n (x_i - \bar{x}) \cdot (y_i - \bar{y})}{\sqrt{\sum_{i=1}^n (x_i - \bar{x})^2 \cdot \sum_{i=1}^n (y_i - \bar{y})^2}} \tag{3}$$

$$\rho_{\text{spearman}} = 1 - \frac{6 \sum_{i=1}^n d_i^2}{n \cdot (n^2 - 1)} \leftrightarrow d_i = \mathcal{R}(x_i) - \mathcal{R}(y_i) \tag{4}$$

where, in Eqs. (3) and (4), n is the number of observations (number of ground motions), x_i is the i^{th} observation's earthquake characteristic quantity (i.e., PGA, PGV, PGD, CAV, or IA), and y_i is the i^{th} observation's peak response, which is either of the following:

$$y_i = \begin{cases} \ddot{u}^{\max} \\ \ddot{u}^{\text{t},\max} \end{cases} \quad (5)$$

Also, in Eq. (4), d_i is the difference between the two ranks of observation x_i and y_i , $\mathcal{R}(x_i)$ returns the rank of x_i in the array of $\{x_1, \dots, x_n\}$, and $\mathcal{R}(y_i)$ returns the rank of y_i in the array of $\{y_1, \dots, y_n\}$.

The Pearson correlation coefficient shows the level of a linear relationship, and Spearman's rank correlation indicates the monotonous connection between the samples and the results. Having both formulas indicating a high correlation implies a strong relationship. In this paper, when both expressions point to a high level of correlation, the connection is elaborated into an empirical function.

3 Ground motion time-histories and structures

In this study, 123 ground motion time-histories are used. These ground motions are instrumental for our research on a plane strain analysis of MRRCFs. To comprehensively explore the seismic response of MRRCFs, we designed eight unique MRRCF models, each characterized by variations in weight, height, and span configurations. This resulted in a total of 984 simulation scenarios. The primary objective of our analysis is to determine the maximum accelerations experienced by these MRRCFs, which is accomplished through inelastic response analysis.

3.1 Earthquake ensemble

Figure 1(a) shows the magnitude-distance distribution of the ground motion time-histories used in this study. The points are also colored by their site conditions, defined by the time-averaged shear-wave velocity – V_{S30} , showing a wide representation of soft to hard soil sites. Note that because this analysis is not oriented at a specific site with specific conditions, the only criteria for choosing time histories was to ensure that variability in site conditions and in-ground motion parameters is well represented, as shown in the GMIM histograms in Fig. 1(b)–1(f). The GMIMs used for analysis in this paper were selected so that they include both peak parameters (PGA, PGV, PGD) and duration-sensitive parameters (CAV, IA). Table 11 in Appendix 0 provides a comprehensive overview of the ground motion time-histories considered in this study. It lists their names and respective years of occurrence, the recording station where data was acquired, and the essential earthquake parameters that appear in Fig. 1(a)–1(f).

We note that 25 of the 123 ground motions are downloaded from the Center for Engineering Strong Motion Data repository (CESMD), and the rest from the Next-generation attenuation (NGA-West2) database, accessible via <https://www.strongmotioncenter.org> and <https://ngawest2.berkeley.edu/>, respectively. The ground motion selection in our dataset spans a wide range of intensities to ensure that our analysis covers a broad spectrum of

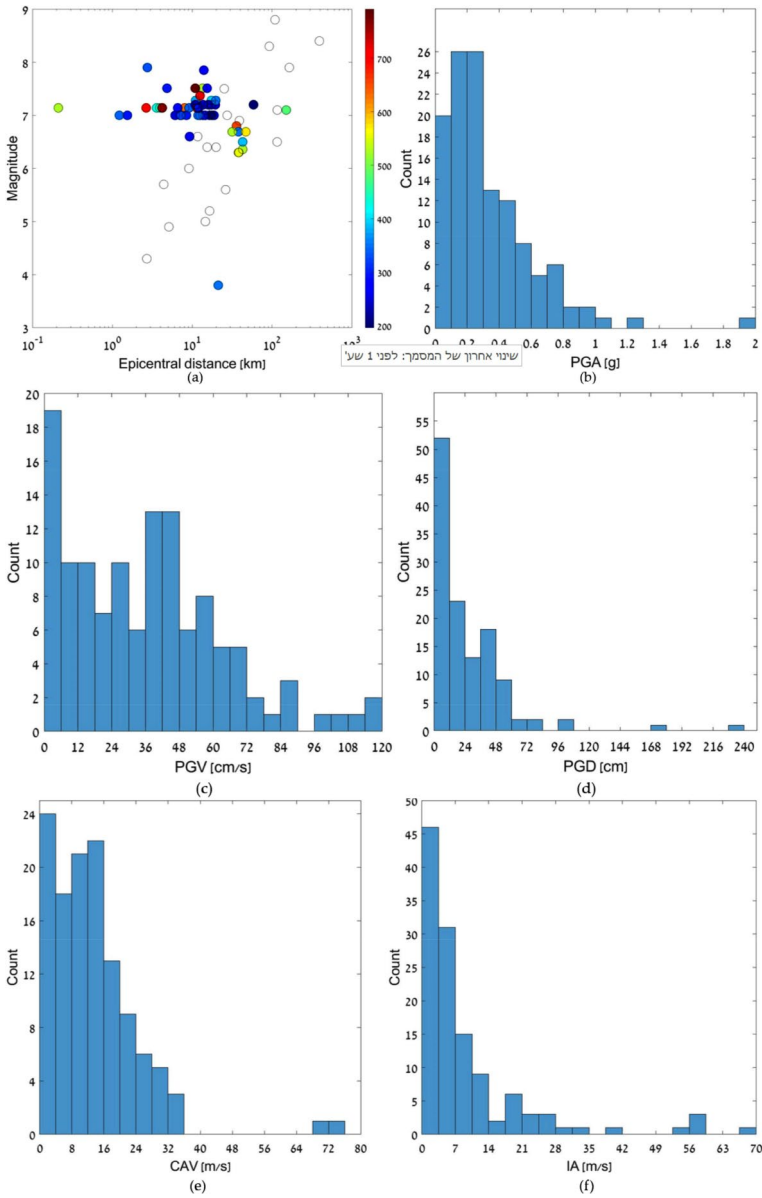


Fig. 1 (a) Scatter of the earthquakes’ magnitude and the epicentral distance; (b) Histogram of the PGA; (c) Histogram of the PGV; (d) Histogram of the PGD; (e) Histogram of the CAV; (f) Histogram of the I_A

seismic responses, enhancing the robustness and applicability of our findings to a more comprehensive range of real-world scenarios.

3.2 Frame models

The study encompasses eight distinct MRRCFs ranging in height from 5 to 45 stories ($N_s = 5-45$, where N_s is the number of stories). These MRRCFs were meticulously designed, following three main criteria:

- (i) The gravitational ceiling load per area is 10.0 kN/m^2 , accounting for service loads, ceiling self-weight, and additional loads.
- (ii) The effective load area is defined such that the highest modal period (the first modal period) equals:

$$T_1 = 0.1N_s$$

- (iii) The applied axial load does not surpass 60% of the columns' cross-sectional capacity.

The MRRCFs are assigned with concrete material properties according to the EN1992-1-1 (2005) standard (see Table 1). The employed concrete types and their strength properties are specified in Table 1. The steel bars are given a characteristic yield strength of 500 MPa and $E = 200 \text{ GPa}$ per the EN1992-1-1 (2005) standard. The geometrical properties are provided by Table 2, which catalogs a total of 17 distinct cross-section design types, each pertaining to the beams and columns within the MRRCFs. These design types specify dimensions, concrete types, steel bar diameters, and steel bar spacing. It is worth noting that the concrete cover and steel bar diameter may exhibit variation between edge and inner columns for specific cross-sectional designs.

The inelastic dynamic response of the MRRCF members (i.e., beams and columns) is analyzed based on the material properties above while considering the stress-strain relationship of EN1992-1-1 for reinforced concrete cross-sections. The column cross-sections are subject to bending, compression, and shear. The Beam cross-sections are subject to bending and shear.

Tables 3, 4, 5, 6, 7, 8, 9 and 10 provide a comprehensive breakdown of the MRRCFs, offering insights into the number of columns, span lengths, effective load areas, and story heights. These tables also outline the assignment of cross-section types to each story within the 5, 10, 15, 20, 25, 30, 40, and 45-story MRRCFs, respectively. Figures 2, 3, 4, 5, 6, 7, 8 and 9 visually depict the modal deformations of the first three modal systems. We acknowledge that the taller MRRCFs, such as the 40 and 45-story variants, may appear unconventional within this system; however, their inclusion in this study serves the purpose of exploring a broader spectrum of system parameters, including fundamental modal periods and sizes.

Table 1 Concrete material properties (EN1992-1-1)

Concrete type	Characteristic cylinder compressive strength [MPa]	Elastic modulus [MPa]	Mean tensile strength [MPa]
C25/30	25	31	2.6
C30/37	30	33	2.9
C35/45	35	34	3.2

Table 2 Types of cross-section types and specifications

Cross-section type #	Structural function	width/height [cm]	Concrete type	Steel bars spacing [cm]	Concrete cover [mm]		Steel bar diameter [mm]	
					Edge	Mid.	Edge	Mid.
1	beam	30/60	C25/30	100	44	44	12	12
2	beam	30/60	C30/37	100	44	44	12	12
3	beam	30/60	C35/45	100	43	43	14	14
4	column	30/60	C25/30	100	44	44	12	12
5	column	40/80	C25/30	100	43	43	14	14
6	column	40/100	C25/30	100	43	43	14	14
7	column	50/100	C25/30	100	43	43	14	14
8	column	50/120	C25/30	100	41	41	18	18
9	column	30/60	C30/37	100	44	37	12	26
10	column	50/80	C30/37	100	43	37	14	26
11	column	40/100	C30/37	100	41	37	18	26
12	column	50/120	C30/37	100	41	37	18	26
13	column	30/60	C35/45	100	43	37	14	26
14	column	40/60	C35/45	100	43	37	14	26
15	column	50/80	C35/45	100	41	37	18	26
16	column	50/100	C35/45	100	41	37	18	26
17	column	50/120	C35/45	100	40	37	20	26

Table 3 MRRCF specifications for $N_s=5$

Number of columns	6		
Spans length [m]	8.00		
Effective load area [m^2]	176.0		
Story height [m]	4.00		
	Stories 1–2	Stories 3–4	Story 5
Beams' cross-section type	1	1	1
Columns' cross-section type	5	5	5
60% of Axial load capacity [kN]	2,496	2,496	2,496
Applied axial load [kN]	1,920	1,152	208

Table 4 MRRCF specifications for $N_s=10$

Number of columns	6		
Spans length [m]	8.00		
Effective load area [m^2]	176.0		
Story height [m]	4.00		
	Stories 1–4	Stories 5–8	Stories 9–10
Beams' cross-section type	1	1	1
Columns' cross-section type	7	5	4
60% of Axial load capacity [kN]	3,900	2,496	1,404
Applied axial load [kN]	3,884	2,276	740

Table 5 MRRCF specifications for $N_s=15$

Number of columns	6		
Spans length [m]	6.00		
Effective load area [m ²]	129.0		
Story height [m]	4.00		
	Stories 1–5	Stories 6–10	Stories 11–15
Beams' cross-section type	1	1	1
Columns' cross-section type	8	6	4
60% of Axial load capacity [kN]	4,680	3,120	1,404
Applied axial load [kN]	4,460	2,870	1,380

Table 6 MRRCF specifications for $N_s=20$

Number of columns	5		
Spans length [m]	6.00		
Effective load area [m ²]	98.4		
Story height [m]	4.00		
	Stories 1–7	Stories 8–14	Stories 15–20
Beams' cross-section type	2	2	2
Columns' cross-section type	12	11	9
60% of Axial load capacity [kN]	6,264	4,176	1,879
Applied axial load [kN]	5,728	3,586	1,584

Table 7 MRRCF specifications for $N_s=25$

Number of columns	5		
Spans length [m]	5.00		
Effective load area [m ²]	82.0		
Story height [m]	4.00		
	Stories 1–10	Stories 11–20	Stories 21–25
Beams' cross-section type	2	2	2
Columns' cross-section type	12	11	9
60% of Axial load capacity [kN]	6,264	4,176	1,879
Applied axial load [kN]	6,215	3,565	1,115

3.3 Inelastic earthquake response

Inelastic earthquake response analysis is performed to assess the floor acceleration within the MRRCF systems. The earthquake response of the planar frame structures considers the inelasticity of the reinforced concrete material, and the columns' inelastic properties stem from the interaction between the axial loading applied to the columns and the consequent yield/ultimate bending moments. These inelastic properties are according to the stress-strain relationships provided by EN1992-1-1 standard. Also, according to Table 6.5 in the ASCE/SEI 41–17 standard (ASCE 2017), the ratio of post-yielding to initial stiffness is considered 0.5 for all members due to the low loading level.

Table 8 MRRCF specifications for $N_s=30$

Number of columns	5		
Spans length [m]	4.00		
Effective load area [m ²]	67.2		
Story height [m]	4.00		
	Stories 1–10	Stories 11–20	Stories 21–30
Beams' cross-section type	2	2	2
Columns' cross-section type	12	10	9
60% of Axial load capacity [kN]	6,264	4,176	1,879
Applied axial load [kN]	6,220	3,940	1,860

Table 9 MRRCF specifications for $N_s=40$

Number of columns	3		
Spans length [m]	4.00		
Effective load area [m ²]	27.2		
Story height [m]	3.00		
	Stories 1–10	Stories 11–25	Stories 26–40
Beams' cross-section type	3	3	3
Columns' cross-section type	16	15	13
60% of Axial load capacity [kN]	6,510	5,208	2,344
Applied axial load [kN]	6,468	4,733	2,243

Table 10 MRRCF specifications for $N_s=45$

Number of columns	3		
Spans length [m]	4.00		
Effective load area [m ²]	27.2		
Story height [m]	3.00		
	Stories 1–10	Stories 11–25	Stories 26–45
Beams' cross-section type	3	3	3
Columns' cross-section type	17	16	14
60% of Axial load capacity [kN]	7,812	6,510	3,125
Applied axial load [kN]	7,493	5,683	3,080

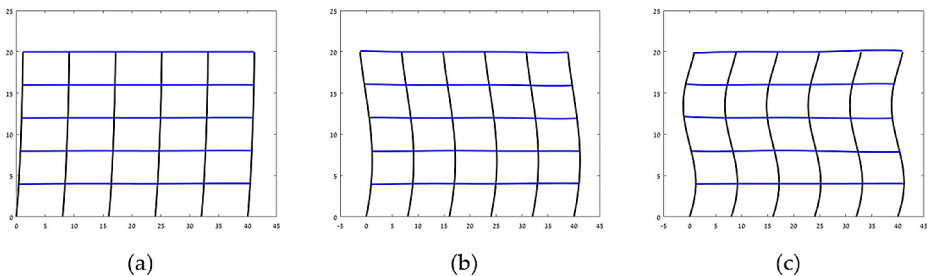


Fig. 2 $N_s=5$ MRRCF modal systems of (a) $T_1=0.5$ s; (b) $T_2=0.135$ s; (c) $T_3=0.063$ s

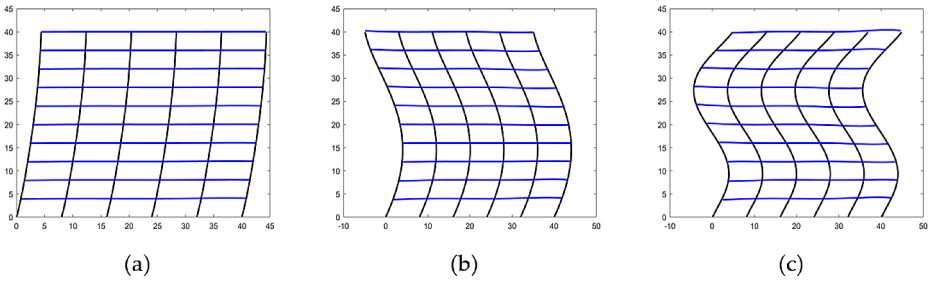


Fig. 3 $N_s=10$ MRRCF modal systems of (a) $T_1=1.0\text{ s}$; (b) $T_2=0.316\text{ s}$; (c) $T_3=0.171\text{ s}$

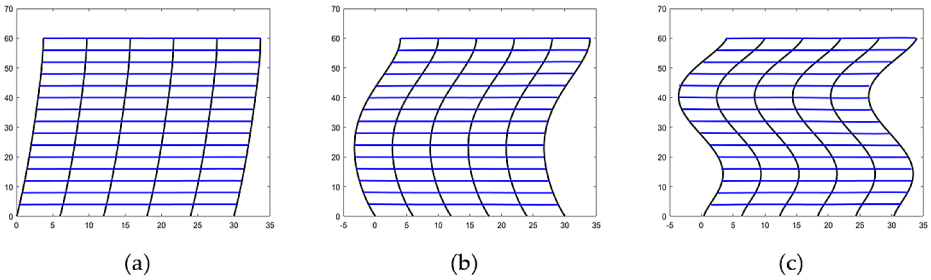


Fig. 4 $N_s=15$ MRRCF modal systems of (a) $T_1=1.5\text{ s}$; (b) $T_2=0.515\text{ s}$; (c) $T_3=0.287\text{ s}$

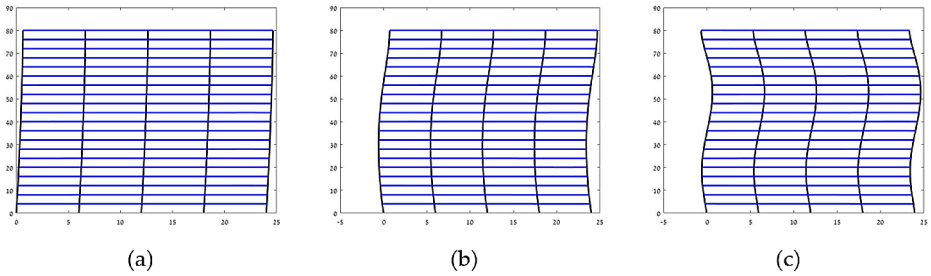


Fig. 5 $N_s=20$ MRRCF modal systems of (a) $T_1=2.0\text{ s}$; (b) $T_2=0.690\text{ s}$; (c) $T_3=0.397\text{ s}$

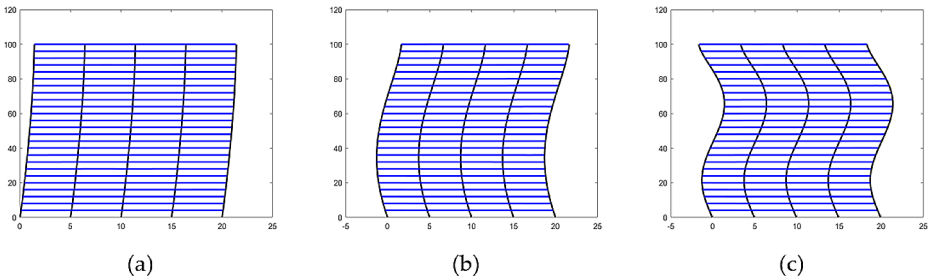


Fig. 6 $N_s=25$ MRRCF modal systems of (a) $T_1=2.5\text{ s}$; (b) $T_2=0.851\text{ s}$; (c) $T_3=0.509\text{ s}$

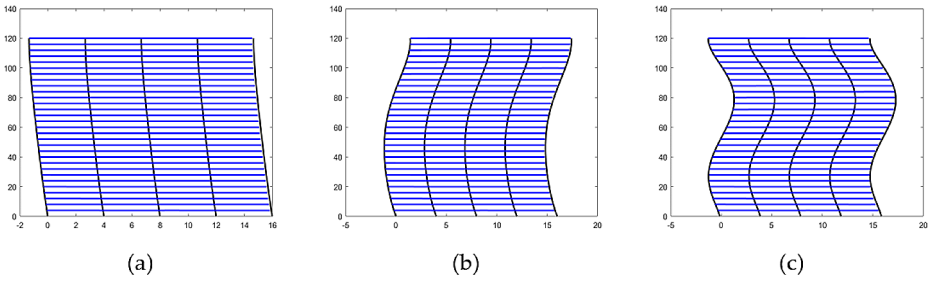


Fig. 7 $N_s=30$ MRRCF modal systems of (a) $T_1=3.0\ s$; (b) $T_2=1.085\ s$; (c) $T_3=0.639\ s$

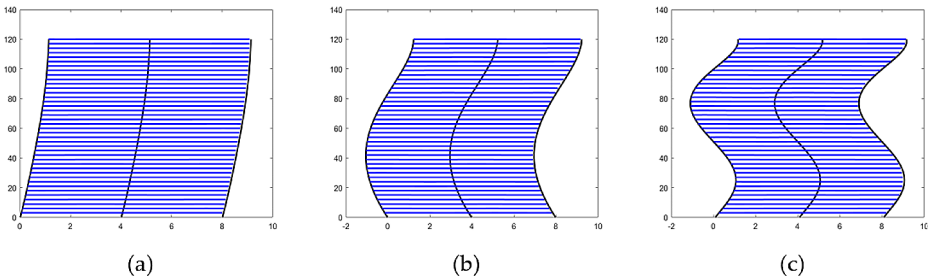


Fig. 8 $N_s=40$ MRRCF modal systems of (a) $T_1=4.0\ s$; (b) $T_2=1.383\ s$; (c) $T_3=0.834\ s$

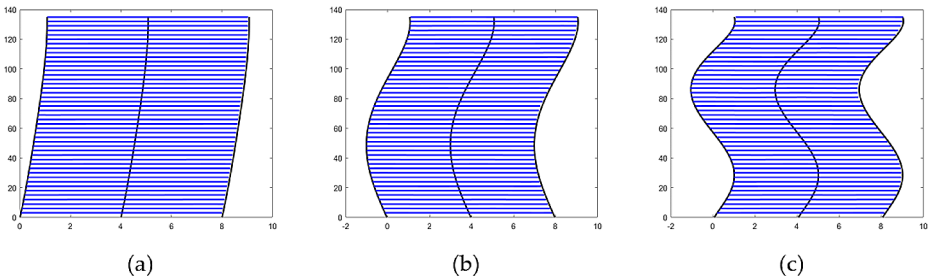


Fig. 9 $N_s=45$ MRRCF modal systems of (a) $T_1=4.5\ s$; (b) $T_2=1.584\ s$; (c) $T_3=0.922\ s$

Numerical evaluation of the inelastic earthquake response is performed using the Newmark- β of constant average acceleration for nonlinear systems, reinforced with the Newton–Raphson method. The tangent stiffness of the planar MRRCF is calculated using the direct stiffness method. The resisting forces of the nonlinear system are analyzed by incorporating the hysteretic model behavior with degradation for deteriorating inelastic structures by Sivaselvan et al. (2000).

It is noted that the vertical axial load applied to the columns does not vary during the numerical simulation due to the over-turning moment. The inelastic properties of the beam stem from the cross-section’s pure bending capabilities. The numerical analysis employs the direct stiffness method in calculating the deformation and resistance of the frame structure. When a column fails (i.e., plastic hinges are formed at both edges), it is assumed that it can

still carry axial load. Hence, the numerical simulation stops when all columns fail at a specific story or the acceleration time-history has ended.

4 Analysis results

This section presents the results of the 8 MRRCF models in section 3.2, loaded with 123 ground motion time-histories presented in section 3.1 (approximately 1,000 simulations total). Almost all of the simulations conducted for this study (98%) entered the structure's plastic range, and some even reached collapse. Figure 10 shows the distribution of structural response in the simulations, categorized into four 'cases': Case A refers to structures that remained elastic throughout the simulation; Case B refers to structures in which at least one element became plastic at some point during the simulation; Case C refers to structures that collapsed (all columns at one story fail) towards the end of the simulation (after time of PGA in the acceleration time-history) and Case D refers to structures that collapsed early in the simulations (before time of PGA). The distribution in Fig. 10 shows that for the $N_s=5, 20, 25,$ and 30 structures, the vast majority of simulations became plastic but did not collapse, while for the $N_s=10, 15, 40,$ and 45 structures, more than 50% of the simulations terminated at structural collapse, but most happened after the time of PGA so that the recorded structural accelerations are still assumed to be representative of maximum structural acceleration.

The distribution of PFA throughout the structure height is presented in Fig. 11, in which all structures ($N_s=5$ through 45) are divided into five sections: the first floor, the lower, middle, and upper thirds, and the upper floor. The results clearly show two patterns of response; while the low structures ($N_s=5$ & 10) experience the maximum floor acceleration at the upper floor, the highest structures ($N_s=40$ & 45) experience the maximum floor acceleration at the bottom floor, and the response of the intermediate structures is something in between. This result can be explained by the fact that the lower the structure, the more

Fig. 10 Earthquake response during simulations: (Case A) structure remained in the elastic range, (Case B) structure entered the plastic range, (Case C) structure collapsed posterior to PGA, (Case D) structure collapsed prior to PGA

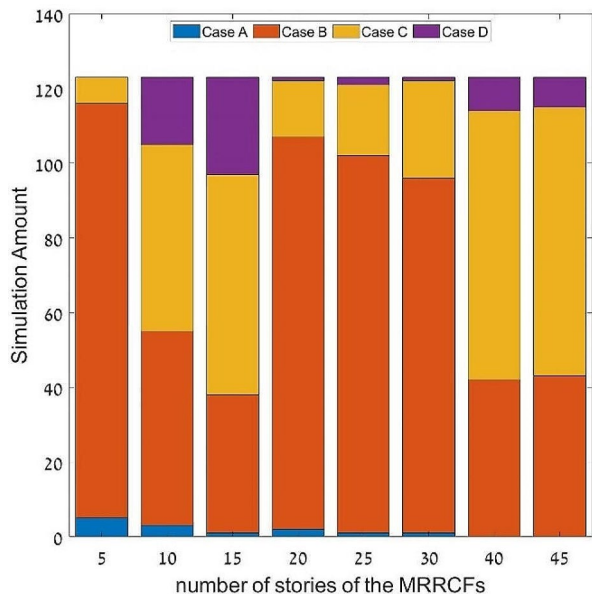


Fig. 11 Distribution of PFA along the height of the structure

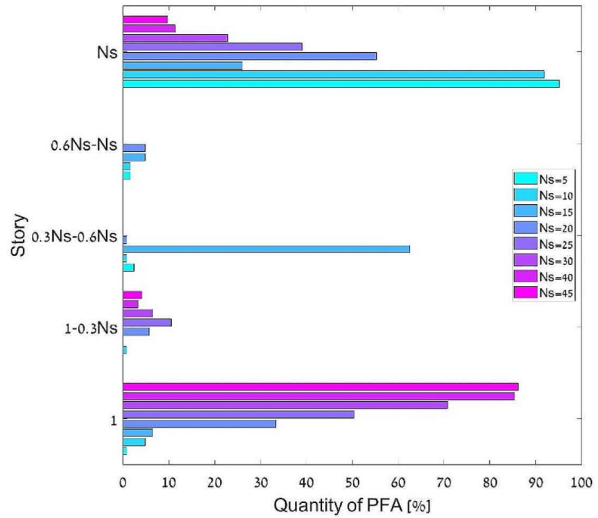
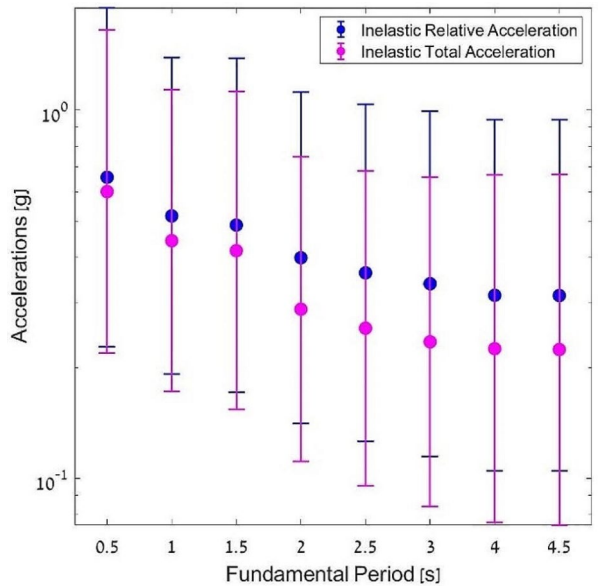


Fig. 12 Range of Inelastic accelerations



dominant the effect of the fundamental period on the total acceleration, and the higher the structure, the more dominant the effect of the shear at the base of the structure.

The distribution of PGA amplitudes for each structure is presented as error bars in Fig. 12. Note that mean and standard deviation are calculated on a log scale, hence the symmetry on the y-axis. While the mean PFA is higher for structures with shorter periods, the obtained standard deviations are about the same for all structures and are primarily dependent on the range of input motions. Hence, we conclude that there is no strong dependence

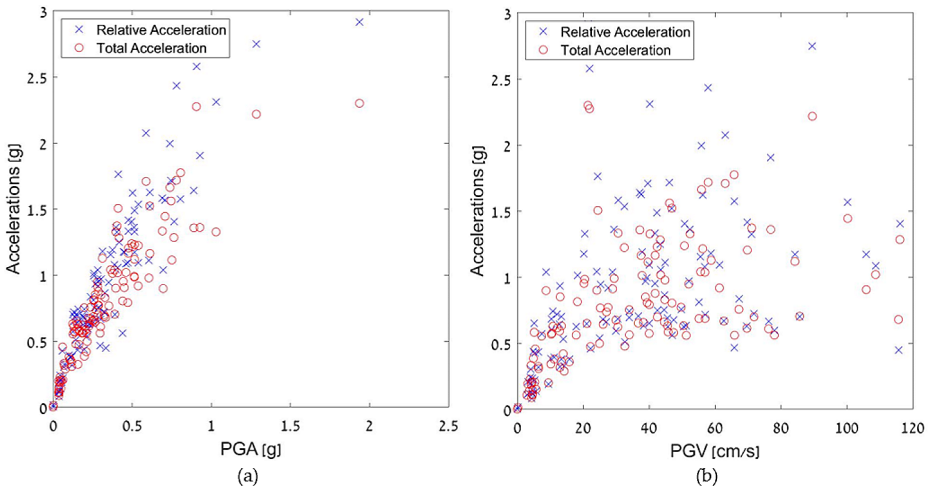


Fig. 13 Scatter of inelastic acceleration and (a) PGA; (b) PGV; of a 5-story building

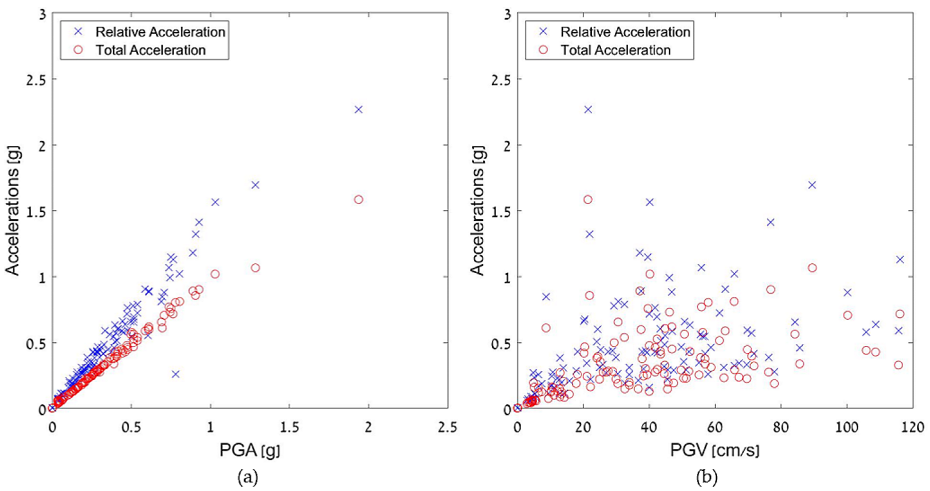


Fig. 14 Scatter of inelastic acceleration and (a) PGA; (b) PGV; of a 45-story building

between the system parameters (such as height, stiffness, and fundamental period) and the resulting PFAs.

Next, we study the correlation between the structural inelastic accelerations and five GMIM—PGA, PGV, PGD, CAV, and I_A . Our research findings unveil a strong association between the accelerations and the PGA. This relationship is exemplified through Figs. 13 and 14 for 5- and 45-story structures, respectively. These figures provide a comparative analysis of structural accelerations, represented on the y-axis, in relation to PGA and PGV, represented on the x-axis. Both structures show a high correlation with PGA, with a clear trend and small scatter, while the trend with PGV is much less distinct, and the scatter is much broader.

Fig. 15 Correlation coefficients between relative inelastic accelerations and GMIM

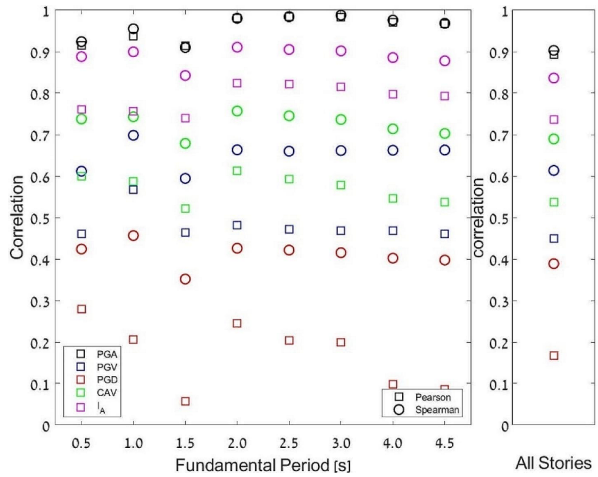
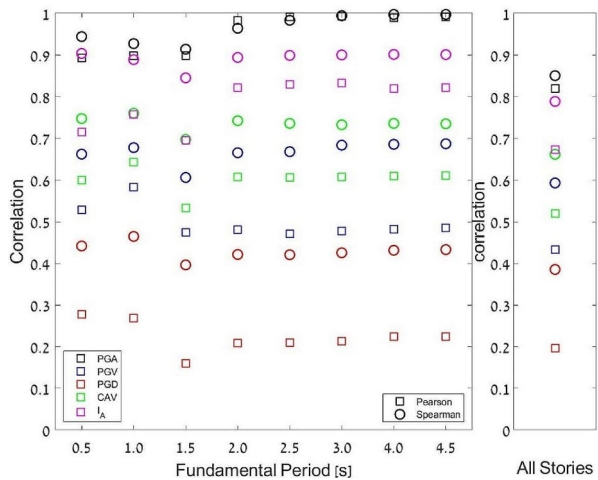


Fig. 16 Correlation coefficients between total inelastic accelerations and GMIM



Figures 15 and 16 show the correlation coefficients between the buildings’ accelerations and five different GMIMs for the relative and the total inelastic accelerations, respectively. In order to avoid assuming that the dependence between the accelerations and the GMIM is linear, in addition to calculating the correlation coefficients according to Pearson, the correlation coefficients were also calculated according to Spearman. These figures show that the correlation between the structural acceleration and PGA is above 0.9 in all cases, followed by I_A , then CAV, and only then PGV and PGD. They also show that except for PGA, the correlation coefficient using Spearman (indicated by circles) is always higher than that with Pearson (marked by squares), suggesting that the correlation is not entirely linear.

5 Suggested model

We suggest a simple parametric model, calculating the total structural acceleration as a function of the structural fundamental period and the PGA. The proposed functional form is as follows:

$$a^{tot} = a \cdot \log(b \cdot PGA + 1) \tag{6}$$

Where the PGA units are in *g*, and the parameters *a* and *b* depend on the fundamental period of the structure, *mp*, using the following terms:

$$a = \begin{cases} 0.85 & mp \leq 1.0 \\ \frac{4}{3} \cdot mp - 0.9 & 1.0 < mp \leq 3.0 \\ 3.10 & 3.0 < mp \end{cases} \tag{7}$$

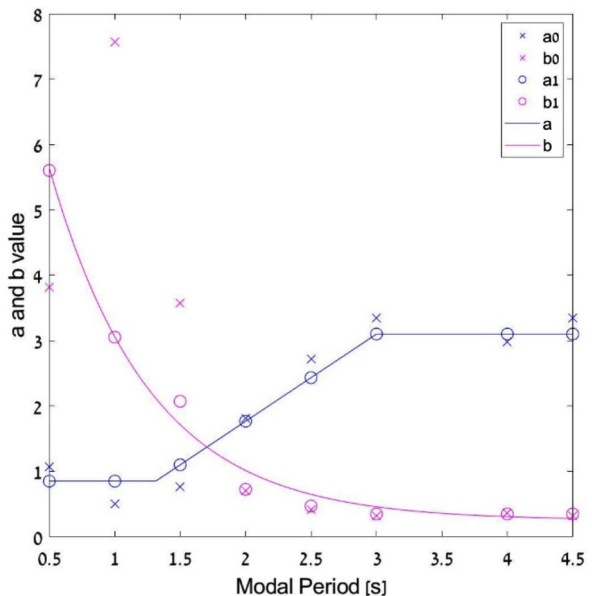
$$b = 10.337 \cdot e^{-1.303 \cdot mp} + 0.25 \tag{8}$$

Equations (7) and (8) relationship with the modal period is depicted in Fig. 17.

The model was developed in two stages to ensure smooth continuous expressions for *a* and *b*, as seen in Fig. 17, *a0* and *b0* are the original coefficients obtained by fitting Eq. (6) with the simulation results, where *a^{tot}* is the maximum acceleration obtained from each simulation. *a1* is a smooth approximation of parameter *a0*, and describes the trend of *a0*, and *b1* is the approximation of parameter *b0*, obtained from solving Eq. (6), with a fixed *a1*. It is worth noting that Eqs. (7) and (8) represent *a1* and *b1* through smooth functions, respectively.

Figure 18(a) and 18(b) compare the accelerations obtained from the analyses with those calculated using the equation proposed in this study for the 5 and 45-story buildings, respec-

Fig. 17 Parameters *a* and *b* versus modal period



tively. The corresponding R-squared values for these structures are 0.856 and 0.907, respectively. With these values, the equations proposed in this study become valuable tools for estimating floor accelerations in MRRCF to protect NSCs.

6 Summary and discussion

The primary objectives of this comprehensive study were to ascertain which parameter has the most substantial effect on the structure's total accelerations during earthquakes and propose a simple parametric model for evaluating the maximum total inelastic acceleration of MRRCF systems. The model is expected to improve the risk assessment of acceleration-sensitive NSCs within MRRCF structures. The data in this paper results from 948 simulations of the eight MRRCFs, with the structure's fundamental period ranging from 0.5 s to 4.5 s, under 123 ground motion time-histories.

While the analysis is believed to be robust and provide significant insight, we recognize a number of limitations which should be acknowledged:

- (i) The analysis is performed in plane strain rather than a full 3D framework. However, we expect the results to be applicable to ordinary three-dimensional structures.
- (ii) The current procedure considers only frame structures, despite those being very rare for >20 stories. However, we prefer to constrain the analysis to one structural type only, at the cost of analyzing slightly non-realistic examples for the higher structures. Also, extending the analysis to 45 stories allows for a more robust estimation at the intermediate heights constrained by higher and lower structures.
- (iii) Vertical ground motions are not considered in the analysis, which is performed in 2D. This simplification is done for two main reasons: (1) in the typical structural analysis focused on structural performance, it is shown that vertical ground motions do not affect ordinary structures but are more significant in the case of longitudinal structures such as bridges. (2) While V/H ratios have been shown to exceed 1.0 at short periods and

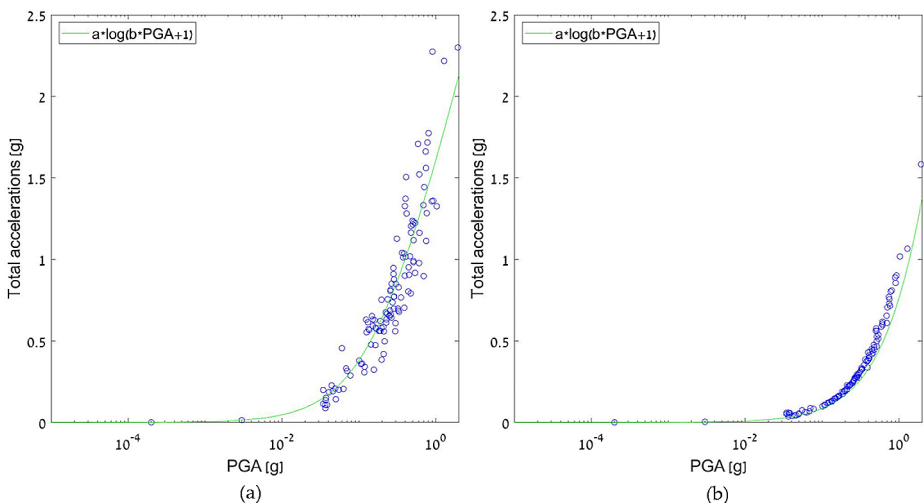


Fig. 18 Total accelerations for a: (a) 5-story building; (b) 45-story building

short source-to-site distances (e.g., Bozorgnia and Campbell 1995, Bradley and Coubri-novski 2011), they typically remain at approximately $V/H=0.5$ elsewhere. Hence, this analysis did not consider vertical ground motions, which are not particularly designed for near-field structures. However, we recognize that significant vertical motions can affect the performance of NSCs and plan to explore that further in future analyses.

The correlation between maximum structural acceleration and several other parameters is quantified using both Pearson and Spearman correlation coefficients. Among the factors analyzed, including fundamental periods, PGA, PGV, PGD, CAV, and IA, it is evident that PGA is the GMIM with the highest correlation to peak total acceleration during earthquakes. We observe that the PFA is primarily observed on high floors in low structures and on low floors in taller structures. Furthermore, a negative correlation exists between PFA and the fundamental period, where longer fundamental periods are suitable with small PFA. The latter correlation will be further elaborated and studied in future research since there seems to be a connection that could be presented through the frequency domain.

Based on these findings, an equation was formulated to determine the total inelastic structural acceleration as a function of both PGA and the fundamental periods of the structure. This development deepens our comprehension of seismic response, aids in structural design considerations, and facilitates risk assessment, ultimately contributing to creating safer built environments.

Appendix

The 123 ground motion time-histories parameters employed in this research are specified in the table below. The ensemble consists of broad parametric samples and a range in terms of Magnitude (Mag.), PGA, PGV, PGD, CAN, and Ariar Inetnsity (I_A) (Appendix Table 11).

Table 11 Ground motion parameters of the ensemble of 123 strong ground motions

EQ. Num.	EQ. Name	Recording station	Mag.	PGA [g]	PGV [cm/s]	PGD [cm]	CAV [m/s]	I_A [m/s]
1	Anchorage 2018	Chugach Park	7.0	1.937	21.45	4.47	35.4	58.1
2	Miyagi 2011	Tsukidate	7.1	1.285	89.55	3,079	32.4	68.4
3	Northern Norcia 2016	Forca Canapine	6.6	0.928	76.93	12.56	16.9	27.4
4	Valparaiso 2017	Torpederas	6.9	0.906	21.95	5.31	23.5	24.9
5	Borrego Springs 2016	Rarick Springs	5.2	0.696	8.75	1.47	3.1	1.6
6	Chile Coquimbo off-shore 2015	El Pedregal	8.3	0.691	30.62	47.15	68.7	58.0
7	South Napa 2014	Main St, Napa	6.0	0.611	46.92	11.95	8.7	6.4
8	Chile 2010	Concepcion San Pedro	8.8	0.606	44.84	31.01	74.3	57.1
9	Calexico 2010	El Centro; Array 11	7.2	0.588	63.11	54.5	29.3	21.9
10	Magna 2020	Lee Kay Center Magna	5.7	0.539	32.5	6.36	5.8	4.9
11	Ridgecrest 2019	Christmas Canyon China Lake	6.4	0.476	41.85	25.97	18.3	9.7

Table 11 Ground motion parameters of the ensemble of 123 strong ground motions

EQ. Num.	EQ. Name	Recording station	Mag.	PGA [g]	PGV [cm/s]	PGD [cm]	CAV [m/s]	I _A [m/s]
12	Ridgecrest 2019	China Lake	7.1	0.444	20.27	7.12	7.5	6.8
13	Ferndale 2010	Ferndale; Fire Station	6.5	0.440	46.97	12.07	9.1	4.2
14	Tallaboa 2020	UUPR	5.6	0.411	24.46	7.36	9.3	5.3
15	Sand Point 2020	Chernabura Island	7.5	0.267	13.04	3.19	15.3	5.2
16	Indios 2020	Ponce	6.4	0.216	24.96	7.33	9.1	2.9
17	Ovalle 2020	Fray Jorge	6.3	0.198	4.92	1.08	2.8	0.6
18	Mina 2020	Monte Cristo Menlo 08	4.3	0.165	5.16	0.56	1.3	0.3
19	Anchorage 2019	Anchorage- Football Stadium	5.0	0.157	6.45	0.37	1.1	0.3
20	Sumatra Aftershock 2007	Sikuai Island	7.9	0.126	7.4	38.54	15.2	3.0
21	La Parguera 2020	PRSN	4.9	0.118	6.49	0.85	0.8	0.1
22	Raboso 2017	Unam	7.1	0.055	9.48	4.14	4.1	0.4
23	Southern Sumatra 2007	Sikuai Island	8.4	0.041	4.2	10.16	4.4	0.3
24	Monte Cristo Range 2020	Lincoln Peak	6.5	0.037	3.6	0.84	2.5	0.1
25	Pollard 2020	Brewton	3.8	0.003	0.22	0.03	0.1	0.0
26	Coalinga	Parkfield cholame 2E	6.36	0.037	5.72	1.43	1.8	0.1
27	Coalinga	Parkfield cholame 2E	6.36	0.0002	0.04	2.77	0.0	0.0
28	Landers	Parkfield Cholame	7.28	0.147	43.41	15.24	11.2	8.7
29	Landers	Parkfield Cholame	7.28	0.284	27.57	18.04	9.2	4.9
30	Landers	Joshua Tree	7.28	0.284	42.50	15.06	17.4	9.4
31	Landers	Joshua Tree	7.28	0.274	27.06	7.81	15.3	6.6
32	Landers	Morongo Valley Fire Station	7.28	0.223	29.96	5.09	13.1	4.8
33	Landers	Morongo Valley Fire Station	7.28	0.164	22.22	10.19	11.1	2.9
34	Northridge	Anaverde Valley City R	6.69	0.060	5.47	1.55	3.0	0.4
35	Northridge	Anaverde Valley City R	6.69	0.044	3.93	1.08	1.6	0.1
36	Northridge	Antelope Buttes	6.69	0.068	4.18	2.15	1.4	0.1
37	Northridge	Antelope Buttes	6.69	0.046	3.20	1.78	1.5	0.1
38	Northridge	Lake Hughes 4B Camp Mend	6.69	0.063	5.34	1.96	1.6	0.1
38	Northridge	Lake Hughes 4B Camp Mend	6.69	0.036	2.93	1.87	1.1	0.1
40	Kocaeli (Turkey)	Arcelik	7.51	0.210	13.95	14.23	4.1	1.2
41	Kocaeli (Turkey)	Arcelik	7.51	0.134	40.05	37.08	3.6	0.9
42	Kocaeli (Turkey)	Duzce	7.51	0.364	55.64	24.95	8.1	5.3
43	Kocaeli (Turkey)	Duzce	7.51	0.312	58.84	43.99	8.5	4.3
44	Kocaeli (Turkey)	Gebze	7.51	0.261	44.6	41.13	5.2	2.2
45	Kocaeli (Turkey)	Gebze	7.51	0.144	32.63	29.76	4.5	1.3
46	Kocaeli (Turkey)	Yarimca	7.51	0.322	71.87	47.32	10.3	5.3
47	Kocaeli (Turkey)	Yarimca	7.51	0.227	69.69	62.30	10.6	5.3
48	Kocaeli (Turkey)	Bolu	7.14	0.806	65.83	13.13	11.7	9.7
49	Kocaeli (Turkey)	Bolu	7.14	0.739	55.90	25.54	14.8	14.9

Table 11 Ground motion parameters of the ensemble of 123 strong ground motions

EQ. Num.	EQ. Name	Recording station	Mag.	PGA [g]	PGV [cm/s]	PGD [cm]	CAV [m/s]	I _A [m/s]
50	Kocaeli (Turkey)	Duzce	7.14	0.515	84.26	47.98	13.4	11.7
51	Kocaeli (Turkey)	Duzce	7.14	0.404	71.15	49.68	13.7	10.8
52	Kocaeli (Turkey)	Lamont1058	7.14	0.107	15.81	8.52	2.8	0.5
53	Kocaeli (Turkey)	Lamont1058	7.14	0.077	14.27	14.38	2.2	0.3
54	Kocaeli (Turkey)	Lamont1059	7.14	0.152	12.86	10.19	5.5	1.5
55	Kocaeli (Turkey)	Lamont1059	7.14	0.137	10.32	8.47	4.7	1.1
56	Kocaeli (Turkey)	Lamont1061	7.14	0.131	12.13	8.79	4.3	1.0
57	Kocaeli (Turkey)	Lamont1061	7.14	0.101	11.19	7.69	4.4	0.9
58	Kocaeli (Turkey)	Lamont1062	7.14	0.259	18.28	8.91	8.6	4.1
59	Kocaeli (Turkey)	Lamont1062	7.14	0.119	10.20	9.02	4.1	0.8
60	Kocaeli (Turkey)	Lamont375	7.14	0.890	37.21	5.04	26.8	39.9
61	Kocaeli (Turkey)	Lamont375	7.14	0.514	20.48	7.46	12.2	8.1
62	Kocaeli (Turkey)	Lamont531	7.14	0.160	10.84	7.65	6.1	1.8
63	Kocaeli (Turkey)	Lamont531	7.14	0.124	13.41	7.91	6.0	1.7
64	Manjil (Iran)	Abbar	7.37	0.515	42.44	15.05	22.2	18.8
65	Manjil (Iran)	Abbar	7.37	0.497	50.73	22.42	31.5	30.0
66	Hector Mine	Hector	7.13	0.328	44.78	10.94	11.8	7.5
67	Hector Mine	Hector	7.13	0.265	26.06	20.06	8.0	3.3
68	Denali (Alaska)	TAPS Pump Station 10	7.9	0.333	115.67	53.44	15.2	7.6
69	Denali (Alaska)	TAPS Pump Station 10	7.9	0.297	65.94	36.68	12.8	4.2
70	Chi-Chi (Taiwan)	TCU057	6.3	0.038	4.63	2.75	1.6	0.1
71	Chi-Chi (Taiwan)	TCU057	6.3	0.034	4.38	3.95	1.6	0.1
72	Chi-Chi (Taiwan)	TCU100	6.3	0.037	4.36	2.18	1.6	0.1
73	Chi-Chi (Taiwan)	TCU100	6.3	0.034	4.64	3.84	1.6	0.1
74	Chuetsu-oki (Japan)	NIG023	6.8	0.050	4.72	2.52	2.7	0.1
75	Chuetsu-oki (Japan)	NIG023	6.8	0.049	4.56	3.22	1.9	0.2
76	El Mayor-Cucapah (Mexico)	Chihuahua	7.2	0.248	38.31	49.18	23.9	8.3
77	El Mayor-Cucapah (Mexico)	Chihuahua	7.2	0.197	34.02	31.21	25.3	9.2
78	El Mayor-Cucapah (Mexico)	Cerro Prieto Geothermal	7.2	0.288	49.73	45.04	26.4	13.0
79	El Mayor-Cucapah (Mexico)	Cerro Prieto Geothermal	7.2	0.286	41.85	31.39	27.4	12.6
80	El Mayor-Cucapah (Mexico)	Michoacan De Ocampo	7.2	0.538	61.35	39.37	33.3	24.4
81	El Mayor-Cucapah (Mexico)	Michoacan De Ocampo	7.2	0.408	43.51	22.00	30.6	19.3
82	El Mayor-Cucapah (Mexico)	RIITO	7.2	0.397	52.45	48.18	25.9	16.0
83	El Mayor-Cucapah (Mexico)	RIITO	7.2	0.376	37.89	21.49	28.6	18.7
84	El Mayor-Cucapah (Mexico)	Ejido Saltillo	7.2	0.152	45.60	38.96	22.5	6.5
85	El Mayor-Cucapah (Mexico)	Ejido Saltillo	7.2	0.148	36.72	38.67	21.4	6.0

Table 11 Ground motion parameters of the ensemble of 123 strong ground motions

EQ. Num.	EQ. Name	Recording station	Mag.	PGA [g]	PGV [cm/s]	PGD [cm]	CAV [m/s]	I _A [m/s]
86	Darfield (New Zealand)	Canterbury Aero Club	7	0.198	47.46	45.73	13.6	3.4
87	Darfield (New Zealand)	Canterbury Aero Club	7	0.186	34.04	32.49	12.0	3.0
88	Darfield (New Zealand)	Christchurch Cashmere High School	7	0.251	21.15	10.66	12.6	4.1
89	Darfield (New Zealand)	Christchurch Cashmere High School	7	0.229	50.48	36.73	12.5	4.4
90	Darfield (New Zealand)	DFHS	7	0.513	29.41	47.68	19.0	11.3
91	Darfield (New Zealand)	DFHS	7	0.472	40.09	20.50	18.6	10.0
92	Darfield (New Zealand)	DSLCL	7	0.257	39.41	34.08	16.6	8.3
93	Darfield (New Zealand)	DSLCL	7	0.237	67.26	81.12	16.3	6.6
94	Darfield (New Zealand)	GDLC	7	0.764	116.09	100.42	19.3	18.0
95	Darfield (New Zealand)	GDLC	7	0.708	100.27	44.65	18.4	18.8
96	Darfield (New Zealand)	HORC	7	0.477	69.82	29.74	15.0	12.3
97	Darfield (New Zealand)	HORC	7	0.450	105.90	52.92	15.0	12.8
98	Darfield (New Zealand)	LINC	7	0.461	108.73	66.63	16.1	10.8
99	Darfield (New Zealand)	LINC	7	0.388	56.95	33.67	15.8	10.9
100	Darfield (New Zealand)	LRSC	7	0.110	13.38	2.99	5.3	0.9
101	Darfield (New Zealand)	LRSC	7	0.070	12.95	8.87	4.6	0.6
102	Darfield (New Zealand)	Papanui High School	7	0.211	51.28	33.36	16.2	5.1
103	Darfield (New Zealand)	Papanui High School	7	0.182	78.02	49.39	16.8	5.2
104	Darfield (New Zealand)	Riccarton High School	7	0.234	62.72	59.4	14.1	4.8
105	Darfield (New Zealand)	Riccarton High School	7	0.190	30.53	19.83	12.7	3.6
106	Darfield (New Zealand)	RKAC	7	0.191	17.89	11.72	8.0	2.0
107	Darfield (New Zealand)	RKAC	7	0.167	10.55	3.62	7.5	1.7
108	Darfield (New Zealand)	ROLC	7	0.39	85.70	107.21	11.7	6.6
109	Darfield (New Zealand)	ROLC	7	0.325	57.00	21.13	11.6	5.8
110	Darfield (New Zealand)	TPLC	7	0.30	76.28	79.43	15.1	5.8
111	Darfield (New Zealand)	TPLC	7	0.208	45.78	40.95	10.9	3.6
112	Duzce (Turkey)	IRIGM 487	7.14	0.303	38.93	20.05	13.3	7.4
113	Duzce (Turkey)	IRIGM 487	7.14	0.282	28.96	16.60	12.3	6.3
114	Duzce (Turkey)	IRIGM 496	7.14	1.030	40.25	18.47	28.8	53.5
115	Duzce (Turkey)	IRIGM 496	7.14	0.751	39.64	14.57	21.1	26.1
116	Duzce (Turkey)	IRIGM 498	7.14	0.396	24.16	17.60	11.8	8.8
117	Duzce (Turkey)	IRIGM 498	7.14	0.353	25.23	17.57	9.5	4.7
118	El Mayor-Cucapah (Mexico)	Westside Elementary School	7.2	0.281	52.05	56.12	19.3	7.8
119	El Mayor-Cucapah (Mexico)	Westside Elementary School	7.2	0.255	55.17	46.86	15.8	4.9
120	New Zealand 2013	RCS2 20	6.6	0.746	46.21	33.35	23.0	32.6
121	New Zealand 2013	RCS2 20	6.6	0.612	37.56	12.46	20.1	24.2
122	New Zealand 2016	WIGC 20	7.85	0.777	57.95	176.51	27.6	18.6
123	New Zealand 2016	WIGC 20	7.85	0.503	56.28	230.29	21.1	9.4

Author contributions All authors contributed to the study conception and design. Parizat Shir, Shmerling Assaf, and Kamai Ronnie performed material preparation, data collection, and analysis. Parizat Shir wrote the first draft of the manuscript, and all authors commented on previous versions. All authors read and approved the final manuscript.

Funding The authors declare that no funds, grants, or other support were received during the preparation of this manuscript.

Open access funding provided by Ben-Gurion University.

Data availability The datasets generated during and analyzed during the current study are available from the corresponding author upon reasonable request.

Declarations

Competing interests The authors have no relevant financial or non-financial interests to disclose.

Open Access This article is licensed under a Creative Commons Attribution 4.0 International License, which permits use, sharing, adaptation, distribution and reproduction in any medium or format, as long as you give appropriate credit to the original author(s) and the source, provide a link to the Creative Commons licence, and indicate if changes were made. The images or other third party material in this article are included in the article's Creative Commons licence, unless indicated otherwise in a credit line to the material. If material is not included in the article's Creative Commons licence and your intended use is not permitted by statutory regulation or exceeds the permitted use, you will need to obtain permission directly from the copyright holder. To view a copy of this licence, visit <http://creativecommons.org/licenses/by/4.0/>.

References

- ASCE (2017) American Society of Civil Engineers. Seismic Rehabilitation of Existing Buildings, ASCE/SEI 41–06
- ASCE (2000) American Society of Civil Engineers, Prestandard and Commentary for the Seismic Rehabilitation of Building, FEMA 356
- Baker JW (2007) Measuring bias in structural response caused by ground motion scaling. *Pac Conf Earthq Eng* 1–6. <https://doi.org/10.1002/eqe>
- Bozorgnia Y, Niazi M, Campbell KW (1995) Characteristics of Free-Field Vertical Ground Motion during the Northridge Earthquake. *Earthq Spectra* 11:515–525. <https://doi.org/10.1193/1.1585825>
- Bradley BA, Cubrinovski M (2011) Near-source strong ground motions observed in the 22 February 2011 Christchurch earthquake. *Seismol Res Lett* 82:853–865. <https://doi.org/10.1785/gssrl.82.6.853>
- Elenas A, Meskouris K (2001) Correlation study between seismic acceleration parameters and damage indices of structures. *Eng Struct* 23:698–704. [https://doi.org/10.1016/S0141-0296\(00\)00074-2](https://doi.org/10.1016/S0141-0296(00)00074-2)
- EN 1992-1-1 (2005) Eurocode 2: design of concrete structures: general rules and rules for buildings. *Br Stand Inst* 668:225
- Fathali S, Lizundia B (2011) Evaluation of current seismic design equations for nonstructural components in tall buildings using strong motion records. *Struct Des Tall Spec Build* 20:30–46. <https://doi.org/10.1002/tal.736>
- Kim SC, White DW (2004) Nonlinear analysis of a one-story low-rise masonry building with a flexible diaphragm subjected to seismic excitation. *Eng Struct* 26:2053–2067. <https://doi.org/10.1016/j.engstruct.2004.06.008>
- NIST (2018) National Institute of Standards and Technology, recommendations for improved seismic performance of nonstructural components. NIST GCR 18–917
- Reinoso E, Miranda E (2005) Estimation of floor acceleration demands in high-rise buildings during earthquakes. *Struct Des Tall Spec Build* 14:107–130. <https://doi.org/10.1002/tal.272>
- Sivaselvan MV, Reinhorn AM (2000) Hysteretic models for deteriorating inelastic structures. *J Eng Mech* 126:633–640
- Taghavi S, Miranda E (2003) Response Assessment of Nonstructural Response Assessment of Nonstructural. Pacific Earthquake Engineering Research Center

- Taghavi S, Miranda E (2004) Estimation of seismic acceleration demands in Building Components, 13 edn. World Conf Earthq Eng Vancouver, BC, Canada 3199
- Wang T, Shang Q, Li J (2021) Seismic force demands on acceleration-sensitive nonstructural components: a state-of-the-art review. *Earthq Eng Eng Vib* 20:39–62. <https://doi.org/10.1007/s11803-021-2004-0>

Publisher's Note Springer Nature remains neutral with regard to jurisdictional claims in published maps and institutional affiliations.